

## Article

# Experimental Analysis of Structures for Trapping SARS-CoV-2-Related Floating Waste in Rivers

Deep Roy <sup>1</sup>, Simone Pagliara <sup>2</sup> and Michele Palermo <sup>1,\*</sup>

<sup>1</sup> DESTEC—Department of Energy, Systems, Territory and Construction Engineering, University of Pisa, 56122 Pisa, Italy; d.roy1@studenti.unipi.it

<sup>2</sup> Department of Civil and Environmental Engineering, Imperial College London, South Kensington, London SW7 2AZ, UK; simo.pagliara@gmail.com or simone.pagliara19@imperial.ac.uk

\* Correspondence: michele.palermo@ing.unipi.it; Tel.: +39-050-221-7929

**Abstract:** Personal protection equipment (PPE, e.g., masks and gloves) related to the severe acute respiratory syndrome coronavirus 2 (SARS-CoV-2) pandemic may represent a significant source of riverine plastic pollution. Several studies were conducted to analyze plastic transport in rivers; however, apparently, none of them systematically investigated the efficiency of countermeasures in trapping/stopping floating plastic and nonwoven fabric materials originating from the above-mentioned PPE. To fill this gap of knowledge and considering the current importance of the topic, the present paper aims at investigating the efficiency of several structure configurations that can be located in both natural and artificial water bodies. To this end, two different efficiencies were defined, i.e., kinematic (for isolated structures) and trapping (for structures in series). Experimental results evidenced that both the kinematic and the trapping efficiencies increase with the Froude number. We also developed empirical equations, which may be applied for predicting the structure efficiency in limiting plastic transport in rivers.



**Citation:** Roy, D.; Pagliara, S.; Palermo, M. Experimental Analysis of Structures for Trapping SARS-CoV-2-Related Floating Waste in Rivers. *Water* **2021**, *13*, 771. <https://doi.org/10.3390/w13060771>

Academic Editor: Luiza Campos

Received: 13 February 2021

Accepted: 8 March 2021

Published: 12 March 2021

**Publisher's Note:** MDPI stays neutral with regard to jurisdictional claims in published maps and institutional affiliations.



**Copyright:** © 2021 by the authors. Licensee MDPI, Basel, Switzerland. This article is an open access article distributed under the terms and conditions of the Creative Commons Attribution (CC BY) license (<https://creativecommons.org/licenses/by/4.0/>).

**Keywords:** hydrodynamics; physical model; plastic transport; SARS-CoV-2

## 1. Introduction

Plastic pollution currently represents one of the most important environmental challenges, since it negatively affects ecosystems, aquatic life, and human health. Plastic is an inexpensive, lightweight, malleable, and durable synthetic organic material made from hydrocarbons, whose popularity soared during the 20th century. At present, plastic is often used for single-use purposes and its annual production is predicted to increase by six times between 2015 and 2050 [1]. Although several research studies assessed plastic pollution in marine environments and raised the awareness of potential damages to oceans, relatively little work has been done on freshwater ecosystems, especially regarding plastic transport dynamics [2]. Indeed, rivers are important vectors of plastic debris to seas and oceans, and their ecosystems are directly affected by this pollution [2]. The first attempts in quantifying plastic debris transport in rivers were done in the 2010s, investigating the variations of plastic debris concentrations over space and time. These focused on major river such as the Thames [3] and the Tamar in the United Kingdom (UK) [4], the Seine in France [5], the Austrian Danube [6], and the Dutch Rhine [7]. On the other hand, complementary to the river case studies, first predictions of plastic debris emissions into seas and oceans were performed by means of modeling approaches [8–10]. These studies represent fundamental contributions since they highlight the geographical distribution of plastic pollution and plastic debris transport.

In order to assess its environmental impact and identify the sources, plastic debris is usually grouped into four main categories according to mean diameter size: nanoplastics, microplastics, mesoplastics, and macroplastics [11]. Note that, depending on the authors, slightly different classifications can be found in the literature [12]. It is noteworthy that

research studies on freshwater plastic pollution have mainly been limited to the nano- and microplastic fractions [13], while only few works focused on meso- and macroplastic debris up until the study conducted by [14]. These previous studies pointed out that the transport and the input of plastic debris in riverine environments are controlled by both natural (e.g., hydrodynamics and morphology) and anthropogenic (e.g., plastic waste production and management) characteristics of the catchments [15–17]. Furthermore, the main portion of freshwater plastic debris is represented by macroplastics [18]. Therefore, it becomes crucial to focus on plastic transport dynamics in order to efficiently tackle water plastic pollution issues. Since its storage and remobilization cycle may last for centuries, it is also important to account for long preservation times [19]. In addition, the recent pandemic originated by the severe acute respiratory syndrome coronavirus 2 (i.e., SARS-CoV-2) led to a dramatic increase in single-use personal protective equipment (PPE) waste, such as disposable face masks made of nonwoven fabrics and latex/plastic gloves [20]. As a consequence of governmental policies to contain the spread of the virus, an enormous amount of medical waste was produced, mainly composed of plastic-based single-use PPE [21]; as an example, Spain and China registered medical waste increments of 350% and 370%, respectively [22]. Although the surface water quality improved during the lockdown due to the closing down of many industries and anthropogenic activities [23,24], the macroplastic pollution in freshwater environments has dramatically increased in the last year. It is worth remarking that masks are made of polypropylene (PP) and polyethylene terephthalate (PET) and gloves are made of nonwoven materials and latex [25–27]. In addition, [28] reported that most of the microplastic microfibers in the Magdalena River, Columbia, originates from the degradation of nonwoven synthetic textiles. Thus, it is reasonable to assume that such items are contributing and will contribute to an increase in the plastic pollution of rivers and oceans.

Some countermeasures were recently developed to intercept plastic elements in rivers. Among others, the nonprofit organization Ocean Cleanup developed a new technology to control plastic transport in rivers [29]. Specifically, they built The Interceptor™, a system that can stop and collect plastic elements in rivers. This system is made of a floating barrier conveying plastic to a solar-powered robot (the Interceptor). In principle, this system can be located in any river and is a suitable solution for limiting plastic transport to the sea. Another solution is represented by the so-called bubble barriers [30]. A bubble screen is originated from a holed tube located diagonally on the bottom of the river/channel. Air bubbles bring plastic elements to the water surface and then to a catchment system at the river side.

However, according to [2], “additional hydrometeorological and hydraulic data are crucial” in order to enhance the understanding of such a complex phenomenon. Therefore, following the success of the mentioned countermeasures and considering the gap of knowledge pointed out by [2], our study aims at investigating the influence of the kinematic flow field on the superficial plastic transport, originated from the degradation of PPE and other plastic materials. To this end, a dedicated model was built, and specific laboratory tests were conducted using both isolated structures and structures located in series. The kinematics of the flow field was analyzed under different hydraulic conditions, which were consistent with mean annual flow conditions occurring in different water bodies in Tuscany (Italy). Laboratory tests showed that the efficiency of isolated structures in limiting the downstream transport of plastic elements slightly depends on the angle of inclination of the structure with respect to the channel wall and on different materials, in the tested range of parameters. Conversely, the efficiency is affected by the average velocity of the approaching flow (i.e., by the approaching Froude number of the flow) and increases in the case of structures disposed in series. Although field data are necessary to validate laboratory results and investigate potential scale effects, this analysis provides some unprecedented and interesting results on the influence of in situ flow conditions on superficial plastic transport in the presence of intercepting barriers.

## 2. Materials and Methods

An experimental campaign was undertaken in the hydraulics laboratory of the University of Pisa using various kinds of trapping structures. The experiments were carried out in a straight channel having the following characteristics: length = 7.6 m, width ( $B$ ) = 0.6 m, and height = 0.5 m. Primarily, two different kinds of structures were tested, i.e., full-width structures (ranging across the entire width of the channel) and partial structures (ranging across partial width of the channel). The full-width structures used in the study were termed  $S_1$ ,  $S_2$ ,  $S_3$ , and  $S_4$  and are shown in Figure 1a–d, respectively. Likewise, the partial structures employed in this study are illustrated in Figure 2. For all the tested configurations, the depth of the submerged part of the structure was approximately equal to 3 mm.

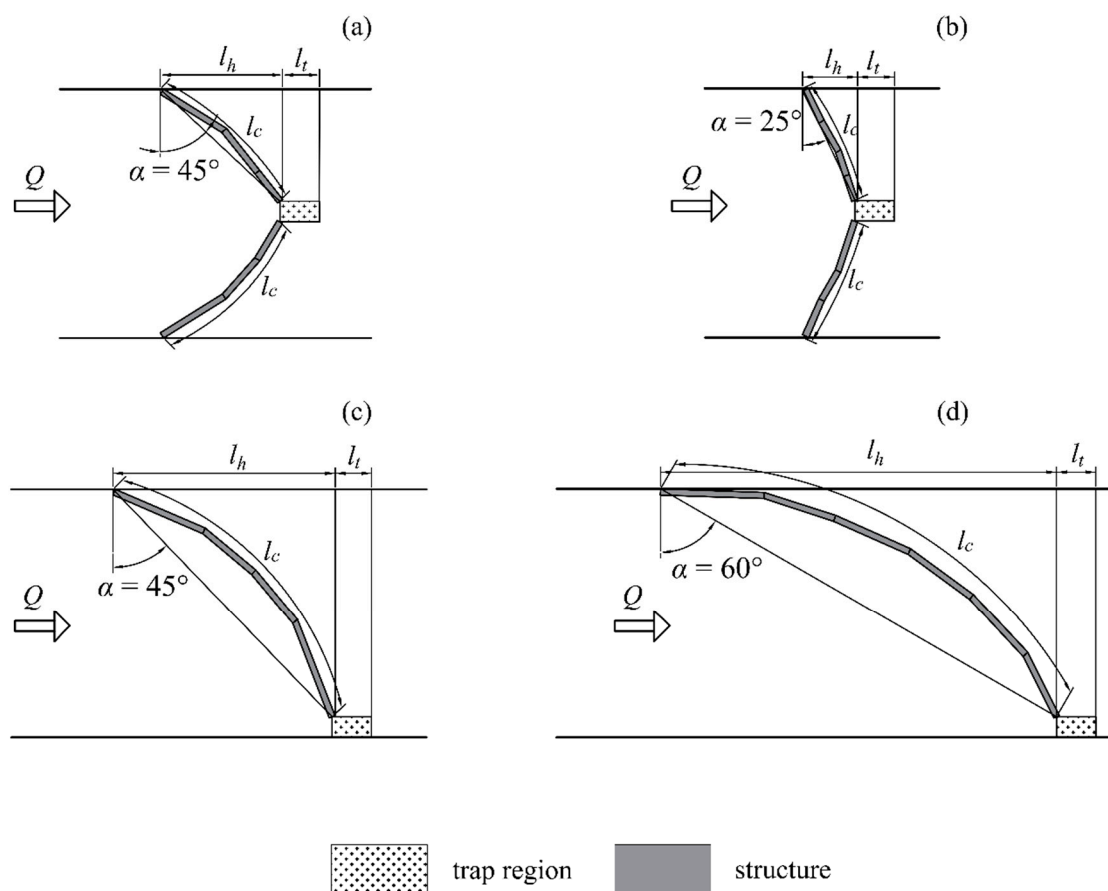


**Figure 1.** Various tested full-width structure configurations: (a)  $S_1$ , (b)  $S_2$ , (c)  $S_3$ , and (d)  $S_4$ .

Figure 1a shows the plan view of  $S_1$  which was characterized by two symmetric arms and a trap region located centrally in the channel to accumulate the material flowing in the river. The trap region consisted of a steel mesh box having a square mouth section whose dimensions were  $0.05 \text{ m} \times 0.05 \text{ m}$  to facilitate the accumulation of floating debris. In Figure 1a,  $l_h/B = 0.48$ , where  $l_h$  is the longitudinal projection of a single arm of the structure. The curved length of one arm of the structure is denoted by  $l_c$  and  $l_c/B = 0.66$ . The angle made by the tangent to the arm of the structure with the transversal direction is defined as  $\alpha$ . In this case,  $\alpha = 45^\circ$ . The flow discharge is denoted by  $Q$ . The nondimensional longitudinal projection of the trap region ( $l_t$ ) is defined as  $l_t/B = 0.16$ . The configuration of the trap was identical for all the tested structures. Figure 1b shows the structure configuration of  $S_2$ , which was also symmetric. However, in this case, the lengths of the arms of the structure were shorter and characterized by  $l_h/B = 0.21$ ,  $l_c/B = 0.5$ , and  $\alpha = 25^\circ$ . Figure 1c,d correspond to structure configurations  $S_3$  and  $S_4$ , respectively, which were asymmetric. These structures were made of a single curved arm ranging across the entire

width of the structure, and the trap region was in the vicinity of the channel bank. In this case,  $l_c$  represents the curved length of the entire arm. The structure configuration  $S_3$  was characterized by  $l_h/B = 0.88$ ,  $l_c/B = 1.33$ , and  $\alpha = 45^\circ$ , whereas the parameters for configuration  $S_4$  were  $l_h/B = 1.6$ ,  $l_c/B = 1.95$ , and  $\alpha = 60^\circ$ .

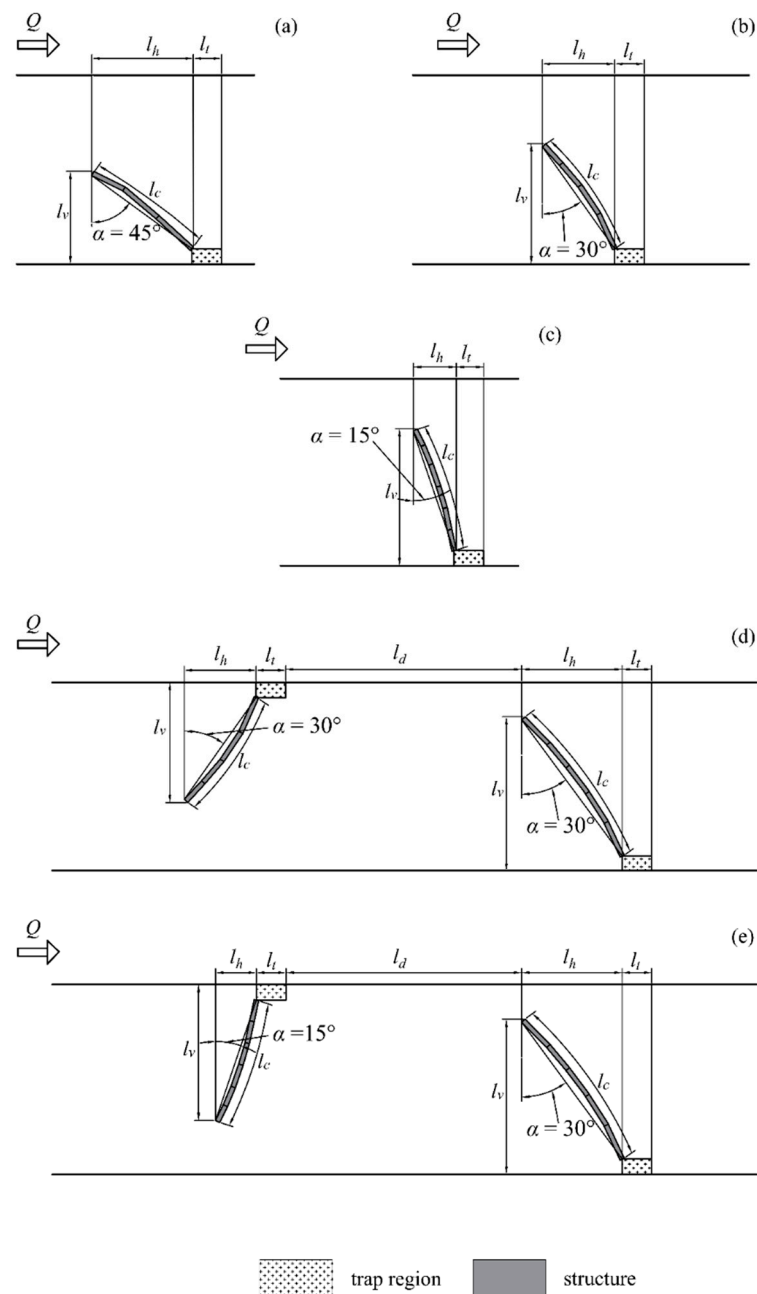


**Figure 2.** Schematic diagram of different structure configurations: (a)  $Sp_1$ , (b)  $Sp_2$ , (c)  $Sp_3$ , (d)  $Sp_4$ , and (e)  $Sp_5$ .

The partial structures used in this study are shown in Figure 2.  $Sp_1$  was an asymmetric structure covering the partial width of the tested channel (Figure 2a). In this case, the trap region was located in the vicinity of the channel bank. This structure configuration was characterized by  $l_h/B = 0.53$ ,  $l_v/B = 0.5$ ,  $l_c/B = 0.66$ , and  $\alpha = 45^\circ$ , with  $l_v$  indicating the length of projection of the structure including the mouth section in the transversal direction of flow. Figure 2b shows the structure configuration  $Sp_2$ , which was characterized by  $l_h/B = 0.4$ ,  $l_v/B = 0.65$ ,  $l_c/B = 0.66$ , and  $\alpha = 30^\circ$ . Similarly, Figure 2c shows the structure configuration  $Sp_3$  ( $l_h/B = 0.23$ ,  $l_v/B = 0.73$ ,  $l_c/B = 0.66$ , and  $\alpha = 15^\circ$ ). In configuration  $Sp_4$ ,

two  $Sp_2$  structures were used in combination separated by  $l_d/B = 1.26$ , where  $l_d$  is the longitudinal distance between the structures in a series arrangement (Figure 2d). Notably, the trap regions of the two structures in combination were in the vicinity of the opposite banks of the channel. The second structure  $Sp_2$  was characterized by a longer arm length ( $l_h/B = 0.53$ ,  $l_v/B = 0.8$ ,  $l_c/B = 0.91$ , and  $\alpha = 30^\circ$ ). Likewise, structure configuration  $Sp_5$  was also tested. This configuration was characterized by a combination of  $Sp_3$  and  $Sp_2$  structures (Figure 2e), where the second structure with  $Sp_2$  configuration had the same characteristics as that in the structure  $Sp_4$ . Pictures of the experimental setups for structure configurations  $S_1$  and  $S_3$  are shown in Figure 3a,b, respectively.

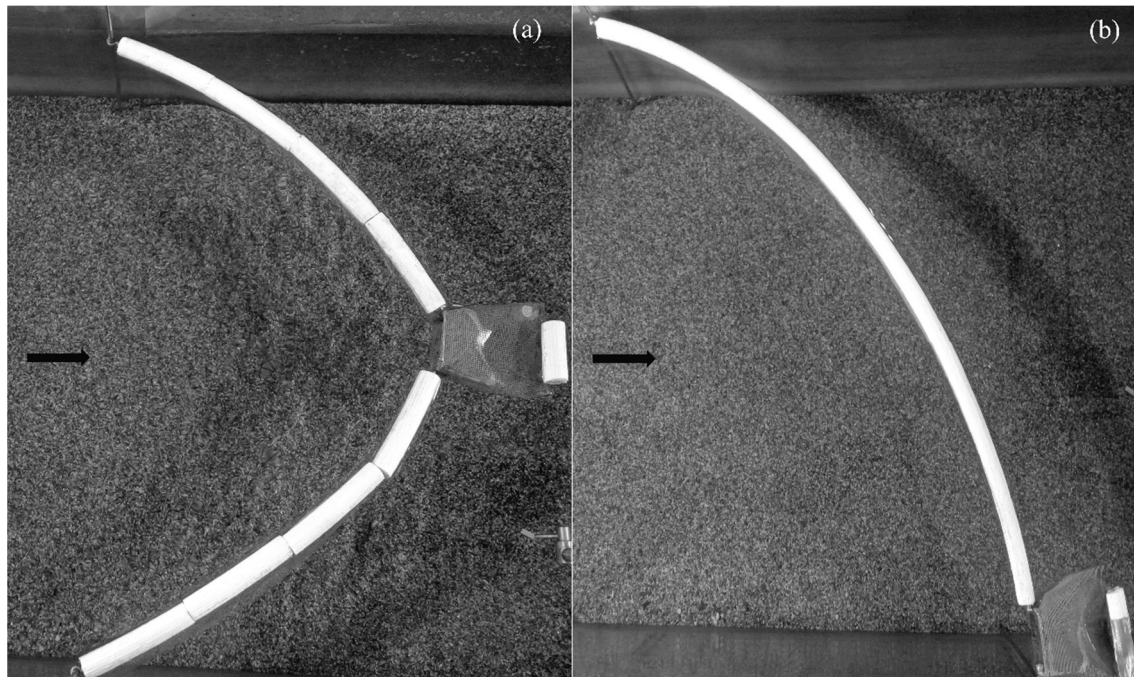


**Figure 3.** Pictures of selected tests conducted with structure configurations (a)  $S_1$  and (b)  $S_3$ . The black arrow indicates the direction of the flow.

The flow characteristics for experimental tests conducted with different structure configurations and in the presence of three main series of plastic and nonwoven fabric materials were measured (using a Nortek acoustic doppler velocimeter (ADV)) and analyzed. The first series consisted of five types of plastic materials that can be commonly found in rivers (originating from bottles, bags, etc.). They were termed as  $P_1$ ,  $P_2$ ,  $P_3$ ,  $P_4$ , and  $P_5$  ( $P$  series) and are shown in Figure 4a–e, respectively. The  $P$  series had an overall density lesser than  $1000 \text{ kg/m}^3$ , i.e., lesser than the water density. The individual plastic elements were either square ( $1.5 \text{ cm} \times 1.5 \text{ cm}$ ) or circular ( $D = 1 \text{ cm}$ ) in shape, where  $D$  is the diameter of the plastic element. They were tested in conjugation with structure typologies  $S_1$ ,  $S_2$ ,  $S_3$ ,  $S_4$ ,  $Sp_1$ ,  $Sp_2$ , and  $Sp_3$ .

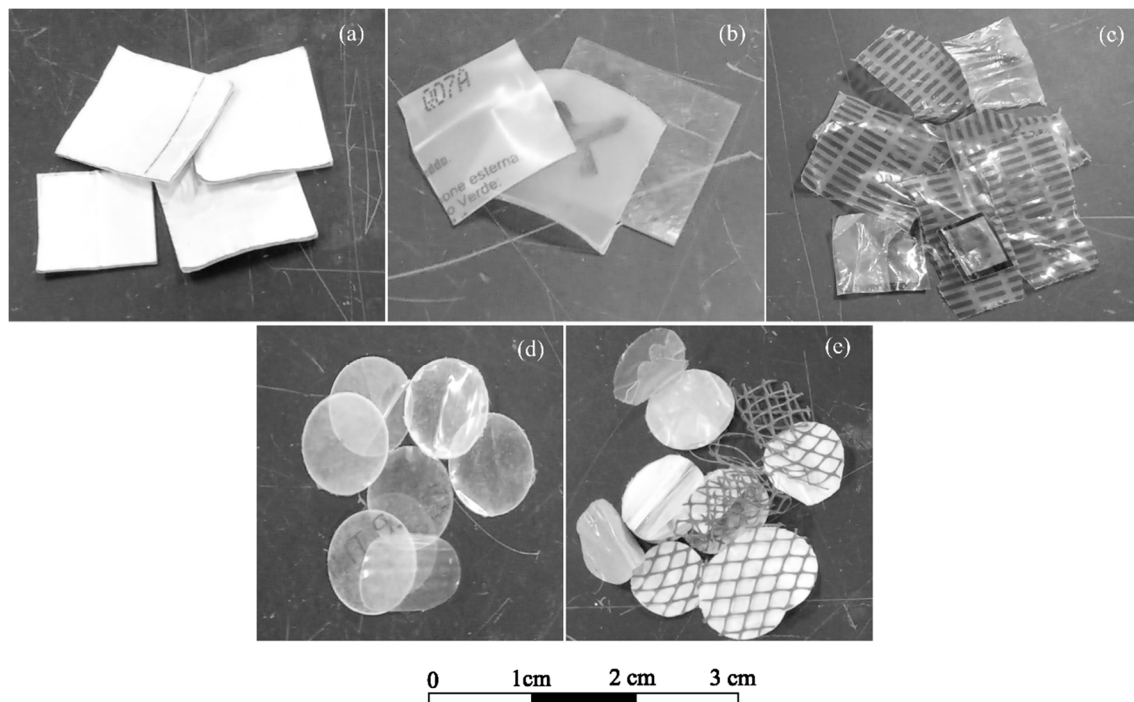


**Figure 4.** Pictures of different types of tested plastic materials belonging to *P* series: (a)  $P_1$ , (b)  $P_2$ , (c)  $P_3$ , (d)  $P_4$ , and (e)  $P_5$ .

Then plastic and nonwoven fabric elements originating from different components of PPE were also tested, particularly masks and gloves. During the pandemic, huge amounts of PPE waste have been generated, representing another potential source of pollution of water bodies. Therefore, plastic from 10 different types of gloves was tested in this study and termed as  $G_1$ ,  $G_2$ ,  $G_3$ ,  $G_4$ ,  $G_5$ ,  $G_6$ ,  $G_7$ ,  $G_8$ ,  $G_9$ , and  $G_{10}$  (*G* series). Lastly, nonwoven fabric materials from seven different types of face masks were tested and denoted by  $M_1$ ,  $M_2$ ,  $M_3$ ,  $M_4$ ,  $M_5$ ,  $M_6$ , and  $M_7$  (*M* series). All the above material types are shown in Figure 5. Like the *P* series, the densities of the materials belonging to the *G* and *M* series were less than  $1000 \text{ kg/m}^3$ . For test purposes, the materials for *G* and *M* series were cut into square pieces ( $1.5 \text{ cm} \times 1.5 \text{ cm}$ ). Thereafter, they were tested in conjugation with structure configurations  $Sp_2$ ,  $Sp_3$ ,  $Sp_4$ , and  $Sp_5$ . The transport of floating material in the channel due to different hydraulic conditions was tested by varying the tailwater and discharge. Table 1 reports the hydraulic conditions, as well as the types of structures and materials used in the different tests, with  $Q$  indicating the discharge,  $h_{tw}$  indicating the water level, and  $v_m$  indicating the average flow velocity in the channel. It is worth noting that the tested range of Froude numbers is consistent with that of some water bodies (e.g., Fiume Morto) in the city of Pisa (Pisa, Italy). Thus, the experimental results of this study can represent a valid aid for future, practical applications.

**Table 1.** Summary of experimental tests.

$Q$ ( $\text{m}^3/\text{s}$ )	$h_{tw}$ (m)	$v_m$ (m/s)	Structure Type (—)	Plastic Type (—)
$0.0100 \leq Q \leq 0.0180$	$0.130 \leq h_{tw} \leq 0.230$	$0.07 \leq v_m \leq 0.21$	$Sp_{2-5}$	<i>G</i> series
$0.0100 \leq Q \leq 0.0180$	$0.130 \leq h_{tw} \leq 0.230$	$0.07 \leq v_m \leq 0.21$	$Sp_{2-5}$	<i>M</i> series
$0.0085 \leq Q \leq 0.0180$	$0.178 \leq h_{tw} \leq 0.285$	$0.05 \leq v_m \leq 0.16$	$S_{1-4}$ , $Sp_{1-3}$	<i>P</i> series



**Figure 5.** Pictures of different types of tested materials belonging to G and M series.

Tests were conducted as follows: primarily, the mobile channel bed was leveled, and water was allowed to enter and reach a desired height. Thereafter, a target discharge  $Q$  was set up, and the water level  $h_{tw}$  was made constant using a sluice gate located at the end of the channel. Then, water level measurements were carried out at selected transversal sections both upstream and downstream of the structure, denoted as 0–0, 1–1, 2–2, and 3–3 (see Figure 6). In each section, measurements were taken at equidistant intervals ( $\Delta y = 10$  cm) in the transversal direction across the entire channel width. Additional measurements were taken along the upstream and downstream contours of the structure, usually around 2.5 cm from the structure (see Figure 6). Following this, in the case of structure configurations  $S_1$ ,  $S_2$ ,  $S_3$ ,  $S_4$ , and  $Sp_2$ , the measurements of flow velocities were taken using a Nortek acoustic doppler velocimeter (ADV) at the selected points at  $z = 1.5$  cm, with  $z$  indicating the depth of the point of measurement from the water surface.

Generally, 15 plastic elements belonging to the  $P$  series were simultaneously released on the water surface 1 m upstream of the structure at equidistant spatial intervals in the transversal direction of the flow across the entire channel width. Their flow pattern was recorded by a high-resolution camera installed above the flume. Their mean velocity at the water surface was estimated from videos and with the help of two measuring tapes attached to both sides of the channel. More specifically, the time taken by macroplastic elements to run across a fixed length was measured in correspondence with the same points upstream of the structure where ADV measurements were taken. This procedure allowed us to estimate the surface velocity magnitude and direction at the selected points. The submerged part of the structure slightly affected measurements taken with the ADV at  $z = 1.5$  cm. Conversely, the surface velocities resulted to be greatly affected by the presence of the structure. Moreover, for each experiment, the percentage of plastic trapped/stopped by the structure was also noted. This allowed obtaining an estimation of the plastic removal

efficiency of each structure, as clarified in a later section. A few special tests were also conducted by mixing plastic elements pertaining to different types of *P* series. Results were found to be consistent with those obtained with plastic elements belonging to single types. Successively, the same methodology was adopted for tests conducted with elements belonging to *G* and *M* series. However, as these tests were essentially conducted using the same range of parameters, ADV measurements were not repeated. However, the analysis of videos also allowed us to estimate the efficiency of the structures in trapping/stopping the floating material. Figure 7a shows a picture of a test conducted with structure configuration  $S_1$  and mixed plastic elements belonging to *P* series. Figure 7b shows the same for a test with structure configuration  $Sp_2$  and plastic type  $G_6$ .

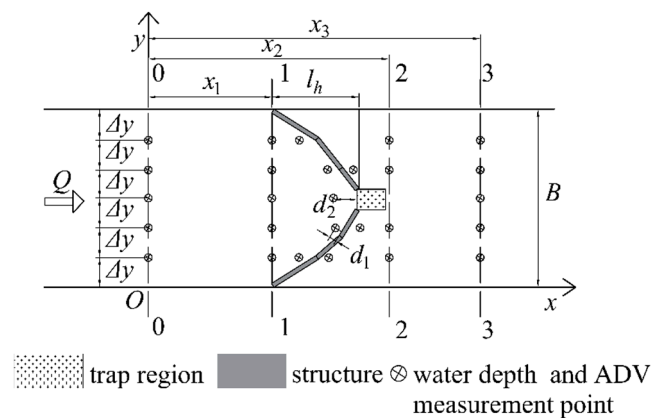


**Figure 6.** Diagram of the test apparatus highlighting water depth and velocity measurement point for structure  $S_1$ .

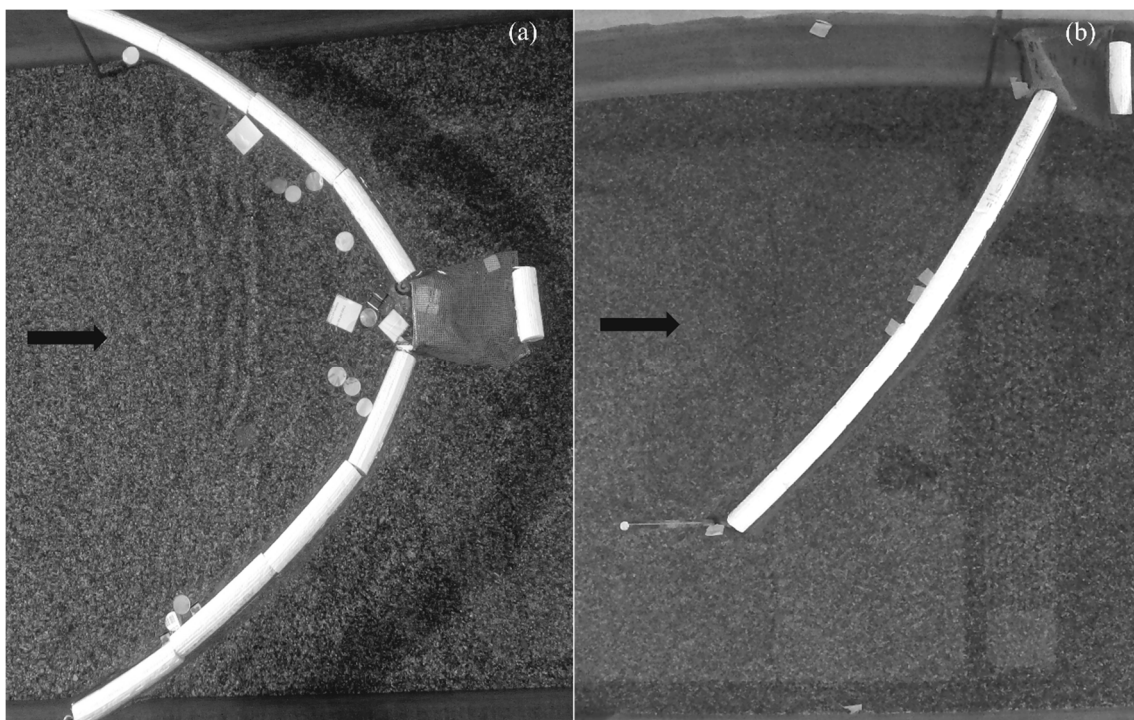


**Figure 7.** Pictures of selected tests conducted with (a) structure configuration  $S_1$  and plastic material belonging to *P* series, and (b) structure configuration  $Sp_2$  and plastic material  $G_6$ . The black arrow indicates the direction of flow.

### 3. Results and Discussion

#### 3.1. Hydrodynamics of Plastic and PPE Equipment at Water Surface

As described in the previous section, ADV measurements were taken 1.5 cm below the water surface ( $z = 1.5$  cm) to estimate the flow velocity characteristics for different tested hydraulic conditions and structure configurations  $S_1$ ,  $S_2$ ,  $S_3$ ,  $S_4$ , and  $Sp_2$ . Furthermore, video analysis allowed us to estimate the mean surface velocity field ( $z = 0$  cm; note that it could not be estimated using the ADV at the water surface). As an example, Figure 8a,b show the flow vectors in the case of  $S_1$  at  $z = 1.5$  cm and 0 cm, respectively. As shown in Figure 8a, the flow velocity vectors approaching the structure were almost exclusively in the  $x$ -direction with a negligible velocity component in the  $y$ -direction (see sections 0–0 and 1–1). The origin of the coordinate system is denoted by O. Likewise, flow measurements along the upstream and downstream contours of the structure revealed a similar behavior for velocity vectors. However, although the velocity vectors at central points at the two sections after the structure, i.e., 2–2 and 3–3, were mainly oriented in the  $x$ -direction, they were also characterized by very small magnitudes. This occurrence was due to the presence of the trap, representing an obstacle for water flow. Conversely, considering the other velocity vectors in sections 2–2 and 3–3, a flow diversion can be pointed out, resulting in vectors on either side of the trap region directed toward the channel bank and characterized by a significant component in the  $y$ -direction.

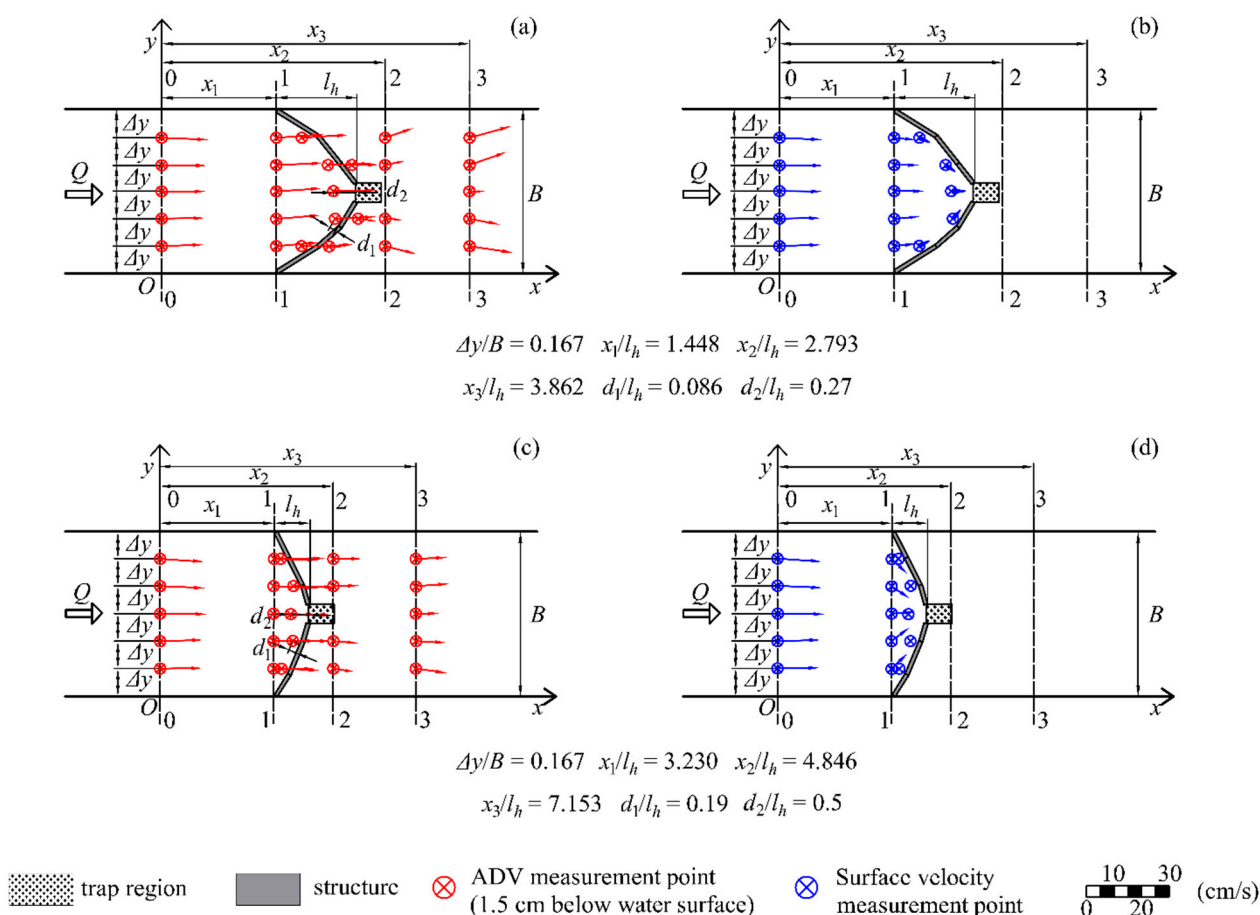


**Figure 8.** Velocity flow field for  $Q = 0.0177$  m<sup>3</sup>/s and  $h_{tw} = 0.186$  m in the case of  $S_1$  at (a)  $z = 1.5$  cm and (b)  $z = 0$  cm, and for  $Q = 0.0179$  m<sup>3</sup>/s and  $h_{tw} = 0.188$  m in the case of  $S_2$  at (c)  $z = 1.5$  cm and (d)  $z = 0$  cm.

With regard to the velocity distribution at  $z = 0$  cm (surface) in the presence of structure configuration  $S_1$  (Figure 8b), a similar vector orientation was observed in the approaching velocity vectors at both sections 0–0 and 1–1. However, moving from section 0–0 to 1–1 and finally to the upstream structure contour, the magnitude of the velocity vectors significantly

decreased because of the flow obstruction due to the structure presence. Nevertheless, close to the structure, the velocity vectors were directed toward the trap region from both sides of the channel. Figure 8c,d show the velocity distribution in the case of structure configuration  $S_2$  at  $z = 1.5$  cm and 0 cm, respectively. Unlike the previous case, the velocity vectors in sections 2–2 and 3–3 downstream of the structure were characterized by a negligible  $y$ -component (Figure 8c). In addition, the magnitude of the velocity vectors at  $z = 0$  cm and in the proximity of the structure was almost equal to zero (Figure 8d). This different behavior was essentially due to the fact that the curvature radius of structure configuration  $S_2$  was bigger than that of  $S_1$ . However, considering that the  $y$ -components of the velocity vectors in the presence of structure  $S_1$  were much smaller than the respective  $x$ -components, an overall similar behavior can be pointed out in terms of plastic transport. Note that such similitude applied to all the tested conditions for structure  $S_1$  and  $S_2$ .

Likewise, we proceeded to analyze the flow velocity distribution due to asymmetric structures  $S_3$  and  $S_4$ . Figure 9a,b show the velocity distributions in the case of structure configuration  $S_3$  at  $z = 1.5$  cm and 0 cm, respectively, whereas Figure 9c,d show the same in the case of structure  $S_4$ . In Figure 9a, the velocity vectors upstream of the structure at 0–0 and 1–1 were mainly directed in the  $x$ -direction with the  $y$ -component almost equal to zero. The same observation also applied to velocity vectors in the vicinity of the upstream contour of the structure. Therefore, the approaching flow distribution due to both symmetric and asymmetric structures was similar at  $z = 1.5$  cm and sections 0–0 and 1–1. However, considering the velocity vectors along the downstream contour of the structure (at sections 2–2 and 3–3), the flow pattern was significantly different from that characterizing symmetric structures. Specifically, the flow was directed toward the channel bank on the opposite side as that of the trap region. Therefore, the velocity vectors downstream of the structure were characterized by significant  $y$ -components. Conversely, the velocity distributions at  $z = 0$  cm (surface) exhibited some similitudes with the case of the symmetric structure (Figure 9b). Specifically, for both tested configurations, the structure posed a significant obstruction to the flow, and the velocity vectors were directed tangentially to the upstream contour of the structure, thus facilitating plastic accumulation. The velocity distribution due to structure  $S_4$  (Figure 9c,d) was essentially similar to that of structure  $S_3$ . The same observations applied to other hydraulic conditions in the presence of asymmetric structures such as  $S_3$  and  $S_4$ .

The velocity distribution due to partial structure type  $Sp_2$  is shown in Figure 10. When the structure spanned a partial width of the channel, there was a considerable impact on the overall velocity distribution. For  $z = 1.5$  cm, the approaching flow velocity was near parallel to the  $x$ -direction in sections 0–0 and 1–1 (Figure 10a). As the flow approached the structure, the flow pattern in the unblocked portion of the channel showed similar characteristics. Nevertheless, in sections 3–3 and 4–4, a mild inclination of the velocity vectors downstream of the structure toward the opposite bank to that of the trap was observed, which is in agreement with the findings in the case of full-width asymmetric structures. In addition, the velocity distribution was asymmetric, resulting in a preferential flow path in correspondence with the unblocked portion of the channel. For  $z = 0$  cm (Figure 10b), the approaching velocity distribution at section 0–0 was directed almost entirely in the longitudinal direction of flow. However, as we moved toward section 2–2, especially in the proximity of the upstream contour of the structure, the velocity vectors were characterized by a significant  $y$ -component, resulting in a portion of the channel in which surface-transported materials escaped from the trapping structure and could move further downstream. Such behavior was found to be similar for all the tested, isolated partial structures, i.e., very slight differences were detected in terms of efficiency in trapping floating material, regardless of the geometric characteristics of the structures.

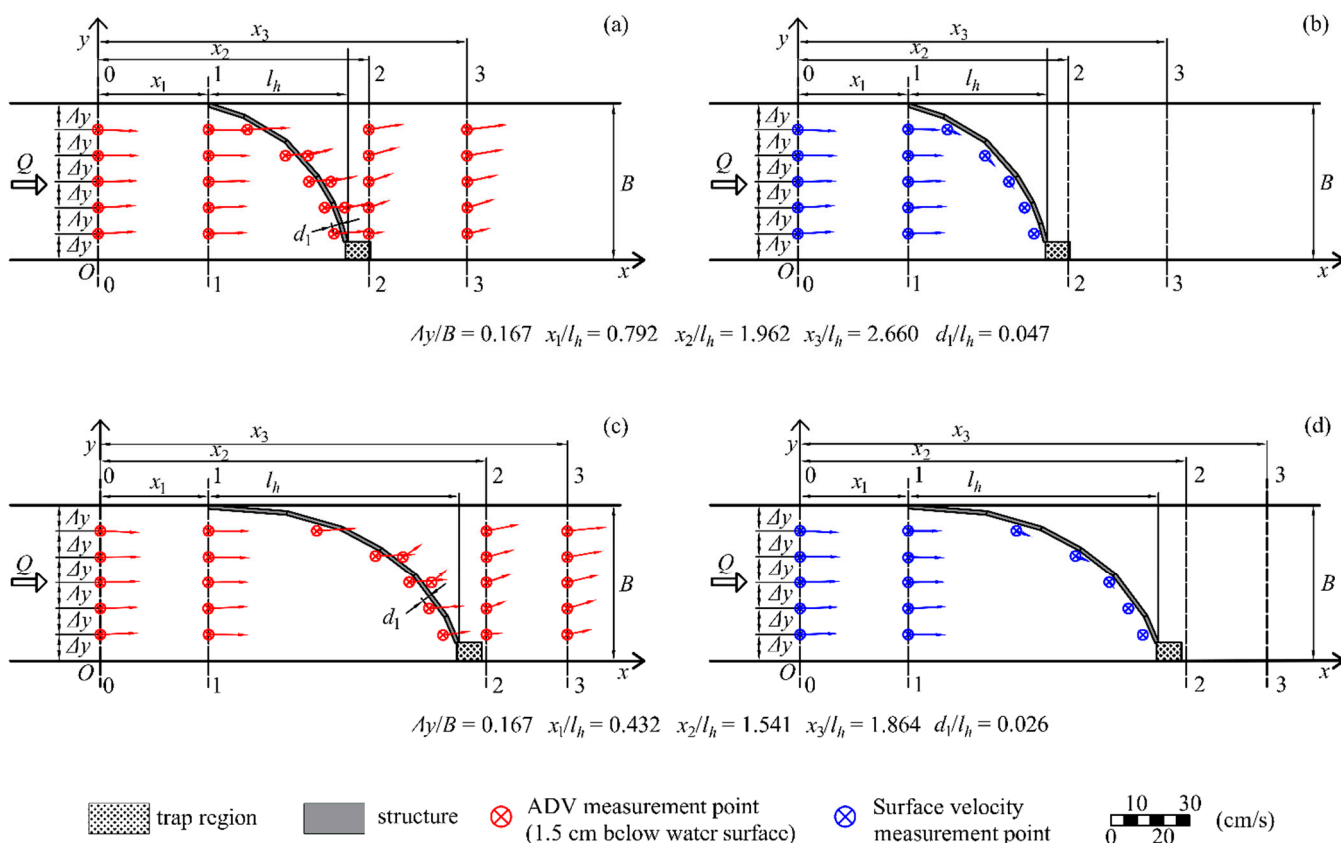


**Figure 9.** Velocity flow field for  $Q = 0.0166 \text{ m}^3/\text{s}$  and  $h_{tw} = 0.178 \text{ m}$  in the case of  $S_3$  at (a)  $z = 1.5 \text{ cm}$  and (b)  $z = 0 \text{ cm}$ , and for  $Q = 0.018 \text{ m}^3/\text{s}$  and  $h_{tw} = 0.2 \text{ m}$  in the case of  $S_4$  at (c)  $z = 1.5 \text{ cm}$  and (d)  $z = 0 \text{ cm}$ .

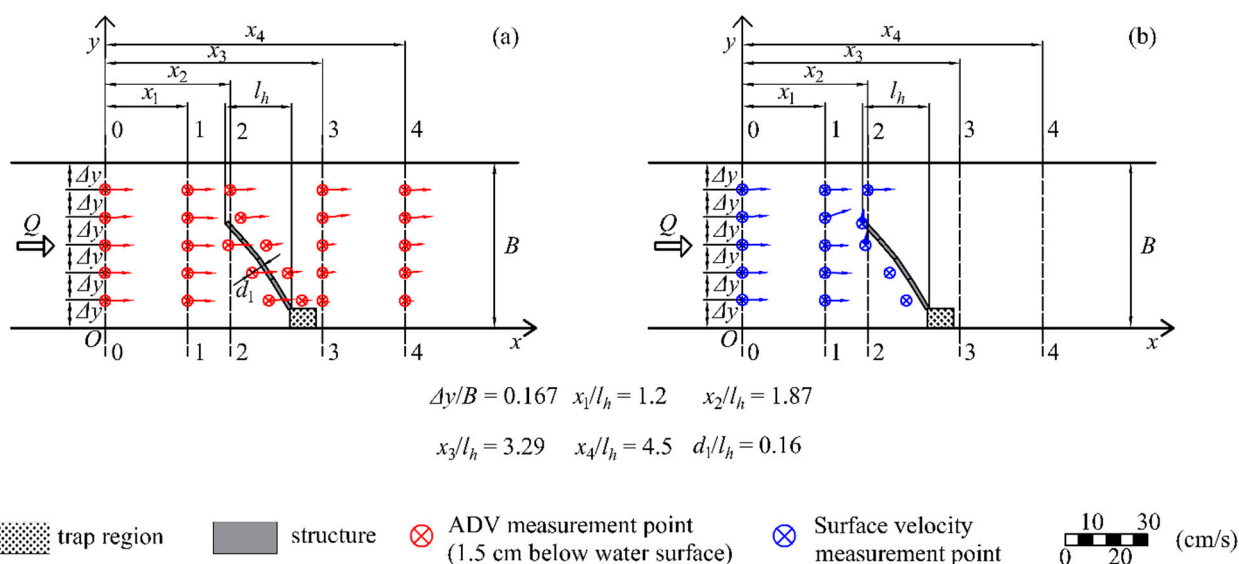


**Figure 10.** Velocity flow field for  $Q = 0.016 \text{ m}^3/\text{s}$  and  $h_{tw} = 0.254 \text{ m}$  for the  $Sp_2$  structure at (a)  $z = 1.5 \text{ cm}$  and (b)  $z = 0 \text{ cm}$ .

Lastly, on the basis of ADV measurements and the analysis of the videos, schematic diagrams of surface streamlines for all tests conducted with partial structure configurations (i.e.,  $Sp_1$ ,  $Sp_2$ , and  $Sp_3$ ) were done in order to provide a qualitative representation of the surface transport dynamics, which was governed by the surface flow characteristics (Figure 11).

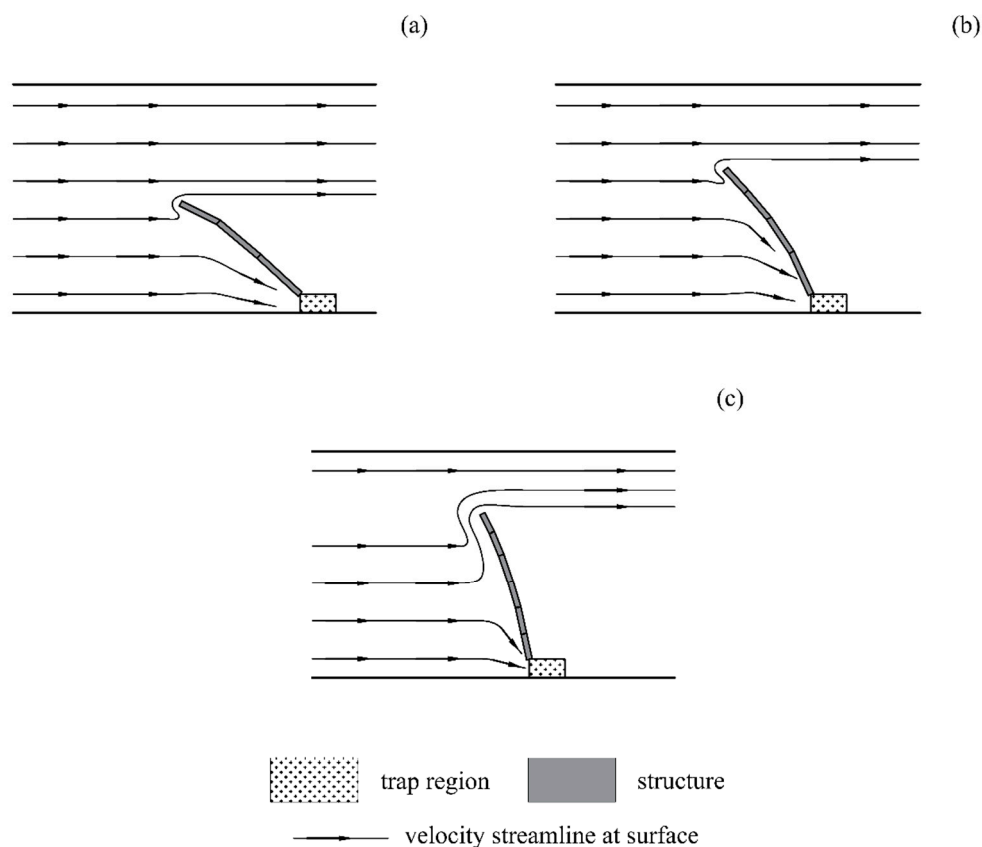


**Figure 11.** Schematic diagrams of surface streamlines for tests conducted with structure configurations (a)  $Sp_1$ , (b)  $Sp_2$ , and (c)  $Sp_3$ .

### 3.2. Kinematic and Trapping Efficiency

In this section, we discuss the efficiency of the isolated, partial structures ( $Sp_1$ ,  $Sp_2$ , and  $Sp_3$ ) and combinations of structures (i.e.,  $Sp_4$  and  $Sp_5$ ) in intercepting the floating material transported on the water surface. It is worth noting that full-width structures such as  $S_1$ ,  $S_2$ ,  $S_3$ , and  $S_4$  could intercept 100% of the floating material, but they represented a barrier that did not allow for navigability of the channel/river where they were located. Therefore, in terms of practical applications, an understanding of the flow dynamics and, consequently, of the efficiency in trapping floating material assumes a fundamental importance in the presence of partial structure configurations. To this end, we first analyzed the behavior of isolated, partial structures, and then we tested their efficiency by considering two combinations of them. Specifically, model measurements and observations revealed that the percentage of floating material (assumed to be distributed uniformly along the transversal direction of the channel) that can be trapped by the structures  $Sp_1$ ,  $Sp_2$ , and  $Sp_3$  was strictly related to the superficial kinematic flow field. In other words, tested materials floating on the portion of the channel in which  $v_y \leq 0$  m/s were intercepted by the structures, with  $v_y$  indicating the  $y$ -component of the velocity vector  $v$  and  $y$  as the transversal axis, directed as in Figure 10. Following these observations, “kinematic” efficiency ( $\eta$ ) can be defined as  $\eta = 100(b/B)\%$ , with  $b$  indicating the width of the portion of the channel where  $v_y \leq 0$  m/s. Likewise, for partial structures located in series ( $Sp_4$  and  $Sp_5$ ), we define the trapping efficiency  $\varepsilon$  as  $\varepsilon = 100(N_t/N)\%$ , with  $N_t$  indicating the number of plastic and PPE pieces intercepted by the structures (counted by using videos), and  $N$  indicating the total number of pieces that were uniformly distributed in the transversal direction upstream of the first structure. Note that, in the case of partial structures located in series, a preferential flow path formed in the unblocked portion of the channel in correspondence with the first structure. Therefore, it is not appropriate to adopt kinematic efficiency, as the flow distribution between the structures was significantly asymmetric.

The analysis of experimental data was conducted in steps. First, we compared the efficiencies  $\eta$  (Figure 12a,b) and  $\varepsilon$  (Figure 12c,d) by testing different materials under various hydraulic conditions, i.e., by varying the inflow conditions represented by the Froude number  $F$ . Overall, it can be observed that, for practical applications, there was no substantial difference in the trend of  $\eta$  for materials belonging to the  $G$  series (Figure 12a). Similar considerations applied to materials pertaining to the  $M$  and  $P$  series (Figure 12b). This occurrence can be explained considering the superficial flow pattern schematically illustrated in Figure 11. Specifically,  $\eta$  only depends on  $b$ , which was found to be a monotonic increasing function of  $F$ , for which the specific material tested had a negligible effect. Furthermore, for higher  $F$  numbers,  $v_y \leq 0$  m/s occurred in a larger portion of the channel due to the flow inertia. Overall, it was found that  $25\% < \eta < 75\%$ , depending on the tested inflow conditions.

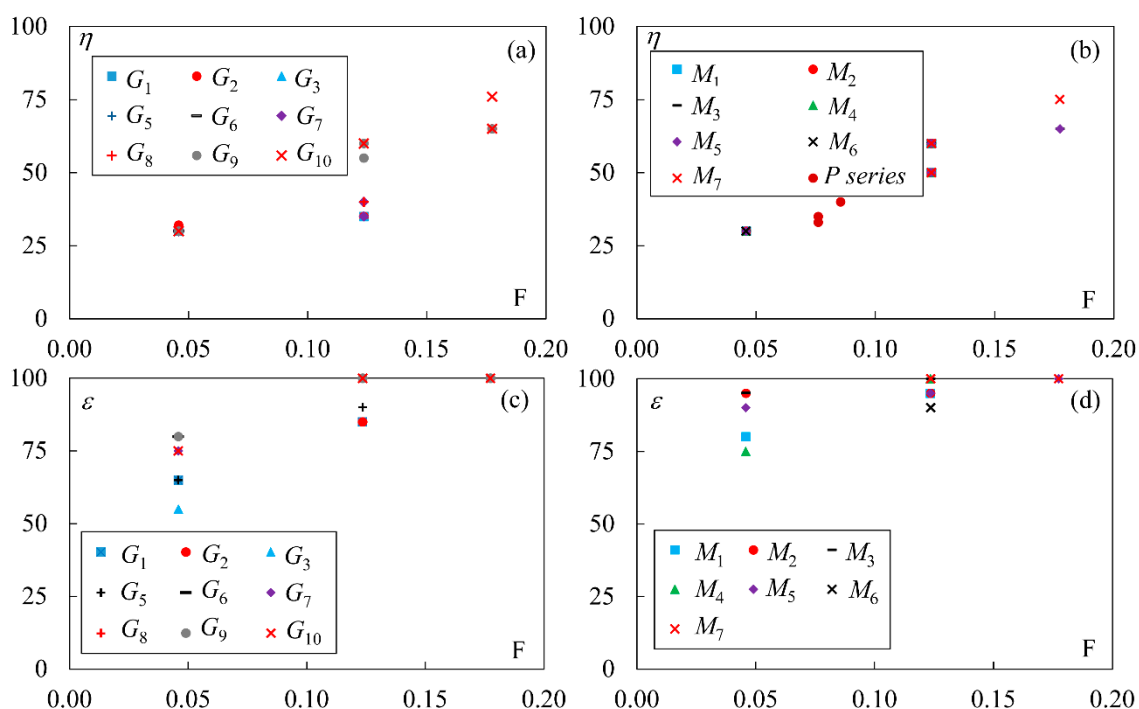


**Figure 12.** Kinematic efficiency  $\eta$  as a function of Froude number  $F$  for tests with materials belonging to (a)  $G$  and (b)  $M$  and  $P$  series. Trapping efficiency  $\varepsilon$  as function of Froude number  $F$  for tests with materials belonging to (c)  $G$  and (d)  $M$  series.

With regard to the estimation of the efficiency  $\varepsilon$ , experimental results confirmed that  $\varepsilon$  can be expressed as a function of the variable  $F$ , and it was not influenced by the tested material pertaining to the same series (Figure 12c,d). It is worth noting that higher Froude numbers resulted in a more asymmetric distribution of flow velocity, i.e., higher velocities (characterized by negligible  $v_y$  components) occurred in the unblocked portion of the channel downstream of the first structure. Therefore, for  $F \geq 0.16$ , all the pieces not intercepted by the first structure were stopped by the second one, resulting in  $\varepsilon = 100\%$ .

A successive analysis was also conducted to detect the effect of the structure typology on both the efficiencies. Experimental data showed that both the efficiencies exhibited the same analytical behavior, regardless of the tested structure typology. Figure 13a,b show two examples of data comparison.

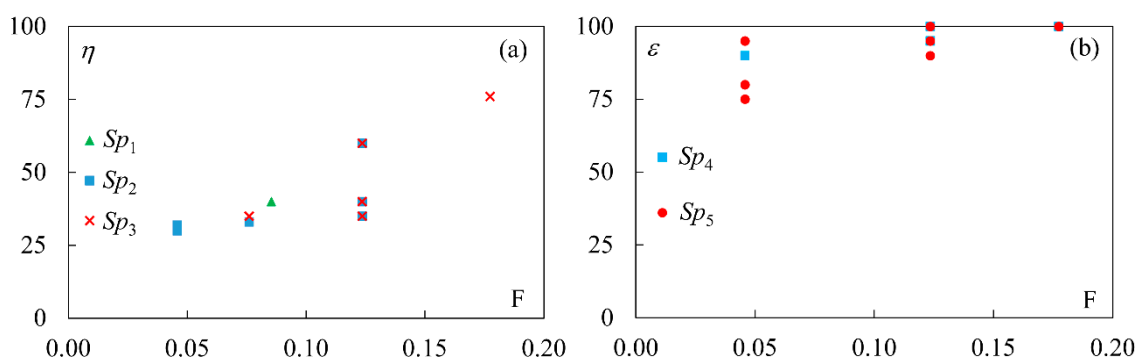


**Figure 13.** (a) Kinematic efficiency  $\eta$  as a function of Froude number  $F$  for tests with structure configurations  $Sp_1$ ,  $Sp_2$ , and  $Sp_3$  and floating materials belonging to series  $G$  and  $P$ . (b) Trapping efficiency  $\varepsilon$  as a function of Froude number  $F$  for tests with structure configurations  $Sp_4$  and  $Sp_5$  and floating materials belonging to series  $M$ .

According to these observations, experimental data were elaborated and the empirical equations below were derived. Specifically, with respect to the kinematic efficiency  $\eta$ , all data can be interpolated using the following linear function (Figure 14a):

$$\eta = 273F + 17 \quad (1)$$

which is valid for  $0.045 \leq F \leq 0.20$ . Similarly, with regard to the trapping efficiency  $\varepsilon$ , we obtained the following (Figure 14b):

$$\varepsilon = 248F + 60.3 \quad (2)$$

which is valid for  $0.045 \leq F < 0.16$  and the  $G$  series, and

$$\varepsilon = 98F + 84.3 \quad (3)$$

which is valid for  $0.045 \leq F < 0.16$  and the  $M$  series. However, considering the relatively slight difference in terms of trapping efficiency  $\varepsilon$  between the two tested series, the following average estimating equation can be adopted for all the cases, regardless of the material typology:

$$\varepsilon = 173F + 72.3 \quad (4)$$

which is valid for  $0.045 \leq F < 0.16$  and both  $G$  and  $M$  series. In addition, for all the tested structures and plastic materials, we obtained

$$\varepsilon = 100 \quad (5)$$

which is valid for  $0.16 \leq F \leq 0.20$ . Note that both  $\varepsilon$  and  $\eta$  are expressed as percentages.

It is worth mentioning that the trapping efficiency  $\varepsilon$  relative to nonwoven fabric material pertaining to the  $M$  series (Equation (3)) was found to be slightly higher than that characterizing data pertaining to the  $G$  series (Equation (2)). This slight difference could be due to the different material composition and structure. Specifically,  $G$  series samples were characterized by a smooth regular surface, whereas those belonging to the  $M$  series were characterized by a certain porosity as they had a net structure. Thus, the water surface tension could have a slight influence on the transport dynamics. However, this phenomenon was not investigated in this study. Likewise, plastic debris items could slip under the barriers at higher flow rates. Thus, further studies are needed in this regard. Nevertheless, this work shows that, for tested hydraulic conditions and configurations, isolated structure efficiency did not depend on structure inclination and plastic material tested. Furthermore, structures disposed in series should be preferred, as they were found to be more effective in intercepting the superficial transport of plastic debris. However, as also noted by [29], no indications on the optimal location of tested structures can be

provided at this stage, as they should be determined on a case-by-case basis, considering the flow and in situ characteristics. Lastly, our results are based on experimental tests conducted in a laboratory flume. Therefore, prototype installations are needed to investigate potential scale effects.

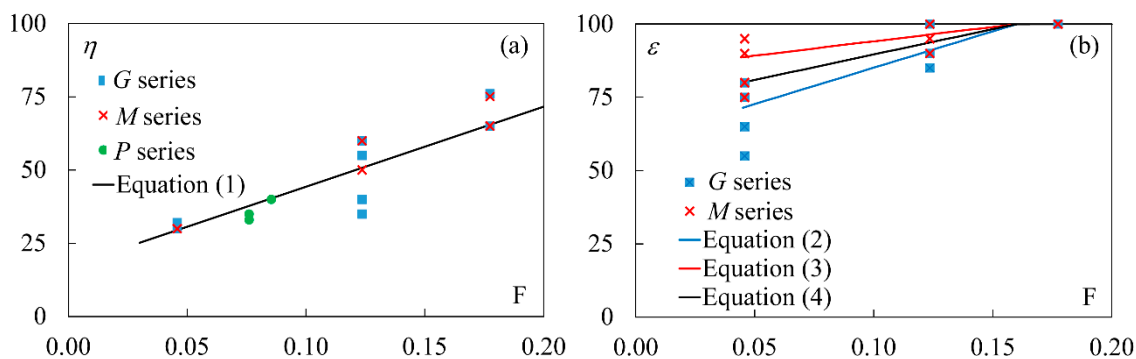


**Figure 14.** (a) Kinematic efficiency  $\eta$  as a function of Froude number  $F$  for all the tests along with the plot of Equation (1). (b) Trapping efficiency  $\varepsilon$  as a function of Froude number for all the tests along with the plots of Equations (2)–(4).

#### 4. Conclusions

In this paper, we analyzed the surface transport of plastic and nonwoven fabric materials in water bodies. To this end, we tested several materials, originating (among others) from plastic bottles, bags, and personal protection equipment (PPE, i.e., masks and gloves used for personal protection during SARS-CoV-2 pandemic). Tests were conducted under different flow conditions and with different control structure configurations. Such structures were tested in order to understand their effect in stopping/trapping the floating material. In particular, we tested two main groups of structures, i.e., full-width structures (ranging across the entire width of the channel) and partial structures (ranging across partial width of the channel). With regard to the partial structures, they were distinguished into isolated structures and structures located in series. For both partial structure configurations, we defined two different efficiencies, i.e., kinematic and trapping. Experimental results showed that both the efficiencies depended on the approaching flow Froude number. Several empirical equations were also derived to estimate the mentioned efficiencies. They represent useful tools to assess the capacity of the tested structure in intercepting the floating material.

**Author Contributions:** Conceptualization, M.P., D.R. and S.P.; methodology, M.P., D.R. and S.P.; validation, M.P., D.R. and S.P.; formal analysis, M.P., D.R. and S.P.; investigation, M.P., D.R. and S.P.; data curation, M.P., D.R. and S.P.; writing—original draft preparation, M.P., D.R. and S.P.; writing—review and editing, M.P., D.R. and S.P.; supervision, M.P. All authors have read and agreed to the published version of the manuscript.

**Funding:** This research received no external funding.

**Institutional Review Board Statement:** Not applicable.

**Informed Consent Statement:** Not applicable.

**Data Availability Statement:** Data used during this study are available from the corresponding author upon request.

**Acknowledgments:** The authors would like to thank the technicians of the hydraulics laboratory of the University of Pisa, Nicola Bruni, Antonio Cecchi, Alessandro Michelotti, and Vincenzo Pennabea, for their help in building the experimental apparatus.

**Conflicts of Interest:** The authors declare no conflict of interest.

## References

1. Zalasiewicz, J.; Gabbott, S.; Waters, C.N. *Plastic Waste: How Plastics Have Become Part of the Earth's Geological Cycle*; Waste, Academic Press: Cambridge, MA, USA, 2019; pp. 443–452.
2. Van Emmerik, T.; Schwarz, A. Plastic debris in rivers. *Wiley Interdiscip. Rev. Water* **2020**, *7*, e1398. [[CrossRef](#)]
3. Morritt, D.; Stefanoudis, P.V.; Pearce, D.; Crimmen, O.A.; Clark, P.F. Plastic in the Thames: A river runs through it. *Mar. Pollut. Bull.* **2014**, *78*, 196–200. [[CrossRef](#)] [[PubMed](#)]
4. Sadri, S.S.; Thompson, R.C. On the quantity and composition of floating plastic debris entering and leaving the Tamar Estuary, Southwest England. *Mar. Pollut. Bull.* **2014**, *81*, 55–60. [[CrossRef](#)] [[PubMed](#)]
5. Gasperi, J.; Dris, R.; Bonin, T.; Rocher, V.; Tassin, B. Assessment of floating plastic debris in surface water along the Seine River. *Environ. Pollut.* **2014**, *195*, 163–166. [[CrossRef](#)] [[PubMed](#)]
6. Lechner, A.; Keckeis, H.; Lumesberger-Loisl, F.; Zens, B.; Krusch, R.; Tritthart, M.; Schludermann, E. The Danube so colourful: A potpourri of plastic litter outnumbers fish larvae in Europe's second largest river. *Environ. Pollut.* **2014**, *188*, 177–181. [[CrossRef](#)]
7. Vriend, P.; Van Calcar, C.; Kooi, M.; Landman, H.; Pikaar, R.; Van Emmerik, T. Rapid assessment of floating macroplastic transport in the Rhine. *Front. Mar. Sci.* **2020**, *7*, 10. [[CrossRef](#)]
8. Lebreton, L.C.M.; Van der Zwet, J.; Damsteeg, J.W.; Slat, B.; Andrady, A.; Reisser, J. River plastic emissions to the world's oceans. *Nat. Commun.* **2017**, *8*, 15611. [[CrossRef](#)]
9. Schmidt, C.; Krauth, T.; Wagner, S. Export of plastic debris by rivers into the sea. *Environ. Sci. Technol.* **2017**, *51*, 12246–12253. [[CrossRef](#)]
10. Liubartseva, S.; Coppini, G.; Lecci, R.; Clementi, E. Tracking plastics in the Mediterranean: 2D Lagrangian model. *Mar. Pollut. Bull.* **2018**, *129*, 151–162. [[CrossRef](#)]
11. Lebreton, L.; Slat, B.; Ferrari, F.; Sainte-Rose, B.; Aitken, J.; Marthouse, R.; Noble, K. Evidence that the Great Pacific Garbage Patch is rapidly accumulating plastic. *Sci. Rep.* **2018**, *8*, 1–15. [[CrossRef](#)]
12. Blettler, M.C.; Ulla, M.A.; Rabuffetti, A.P.; Garello, N. Plastic pollution in freshwater ecosystems: Macro-, meso-, and microplastic debris in a floodplain lake. *Environ. Monit. Assess.* **2017**, *189*, 581. [[CrossRef](#)]
13. Blettler, M.C.; Abrial, E.; Khan, F.R.; Sivri, N.; Espinola, L.A. Freshwater plastic pollution: Recognizing research biases and identifying knowledge gaps. *Water Res.* **2018**, *143*, 416–424. [[CrossRef](#)]
14. Van Emmerik, T.; Schwarz, A. Riverine Macroplastics and How to Find Them. In *EGU General Assembly Conference Abstracts*; European Geosciences Union: Munich, Germany, 2020; p. 11840.
15. Hurley, R.; Horton, A.; Lusher, A.; Nizzetto, L. *Plastic Waste in the Terrestrial Environment*; Plastic Waste and Recycling, Academic Press: Cambridge, MA, USA, 2020; pp. 163–193.
16. Nihei, Y.; Yoshida, T.; Kataoka, T.; Ogata, R. High-Resolution Mapping of Japanese Microplastic and Macroplastic Emissions from the Land into the Sea. *Water* **2020**, *12*, 951. [[CrossRef](#)]
17. Winton, D.J.; Anderson, L.G.; Roccliffe, S.; Loiselle, S. Macroplastic pollution in freshwater environments: Focusing public and policy action. *Sci. Total Environ.* **2020**, *704*, 135242. [[CrossRef](#)]
18. Van Emmerik, T.; Strady, E.; Kieu-Le, T.C.; Nguyen, L.; Gratiot, N. Seasonality of riverine macroplastic transport. *Sci. Rep.* **2019**, *9*, 1–9.
19. Liro, M.; Emmerik, T.V.; Wyzga, B.; Liro, J.; Mikuš, P. Macroplastic storage and remobilization in rivers. *Water* **2020**, *12*, 2055. [[CrossRef](#)]
20. Singh, N.; Tang, Y.; Zhang, Z.; Zheng, C. COVID-19 waste management: Effective and successful measures in Wuhan, China. *Resour. Conserv. Recycl.* **2020**, *163*, 105071. [[CrossRef](#)] [[PubMed](#)]
21. Ammendolia, J.; Saturno, J.; Brooks, A.L.; Jacobs, S.; Jambeck, J.R. An emerging source of plastic pollution: Environmental presence of plastic personal protective equipment (PPE) debris related to COVID19 in a metropolitan city. *Environ. Pollut.* **2021**, *269*, 116160. [[CrossRef](#)] [[PubMed](#)]
22. Klemeš, J.J.; Van Fan, Y.; Tan, R.R.; Jiang, P. Minimising the present and future plastic waste, energy and environmental footprints related to COVID-19. *Renew. Sustain. Energy Rev.* **2020**, *127*, 109883. [[CrossRef](#)]
23. Yunus, A.P.; Masago, Y.; Hijioka, Y. COVID-19 and surface water quality: Improved lake water quality during the lockdown. *Sci. Total Environ.* **2020**, *731*, 139012. [[CrossRef](#)] [[PubMed](#)]
24. Arif, M.; Kumar, R.; Parveen, S. Reduction in Water Pollution in Yamuna River Due to Lockdown under COVID-19 Pandemic. Available online: <https://www.thepharmajournal.com/archives/2020/vol9issue12/PartB/9-11-85-669.pdf> (accessed on 10 March 2021).
25. Silva, A.L.P.; Prata, J.C.; Walker, T.R.; Duarte, A.C.; Ouyang, W.; Barcelò, D.; Rocha-Santos, T. Increased plastic pollution due to COVID-19 pandemic: Challenges and recommendations. *Chem. Eng. J.* **2020**, *405*, 126683. [[CrossRef](#)] [[PubMed](#)]
26. Ajmeri, J.R.; Ajmeri, C.J. *Nonwoven Materials and Technologies for Medical Applications*; Woodhead Publishing Limited: Cambridge, UK, 2011.
27. Martinez Silva, P.; Nanny, M.A. Impact of microplastic fibers from the degradation of nonwoven synthetic textiles to the Magdalena River water column and river sediments by the city of Neiva, Huila (Colombia). *Water* **2020**, *12*, 1210. [[CrossRef](#)]

- 
28. Prata, J.C.; Silva, A.; Walker, T.R.; Duarte, A.C.; Rocha-Santos, T.A.P. COVID-19 pandemic repercussions on the use and management of plastics. *Environ. Sci. Technol.* **2020**, *54*, 1–6. [[CrossRef](#)] [[PubMed](#)]
  29. The Ocean Cleanup. Available online: <https://theoceancleanup.com/> (accessed on 6 March 2021).
  30. The Great Bubble Barrier. Available online: <https://thegreatbubblebarrier.com/en/> (accessed on 6 March 2021).